A novel method for quantifying localised correlation of late-gadolinium intensity with conduction velocity

Rheeda L Ali, Chris D Cantwell , Caroline H Roney, Norman A Qureshi, Phang Boon Lim, Jennifer H Siggers, Spencer J Sherwin, Nicholas S Peters

Imperial College London, United Kingdom

Abstract

Patient-specific computer models of the human atria have the potential to aid clinical intervention in the treatment of cardiac arrhythmias. However, quantifying and integrating the heterogeneous qualities of the myocardium through imaging is particularly challenging due to the unknown relationship between voxel intensity and tissue conductivities. We establish a method to determine the relationship between local conduction velocity and scar density, extracted through the analysis of late-gadolinium enhanced magnetic resonance imaging data.

1. Introduction

Regular propagating electrical wavefronts in the heart are essential for the co-ordinated contraction of cardiac muscle. Cardiac arrhythmias are the result of interruptions to the regular electrical signal, causing irregular contractions or fibrillation of the heart muscle. In the atria this condition leads to reduced cardiac throughput and increases the risk of complications such as stroke. Atrial fibrillation (AF) is the most common type of arrhythmia, affecting over 10% of the over 75 population [1].

Current treatments for AF include radio frequency (RF) catheter ablation, where RF energy is delivered to the cardiac tissue through a catheter, creating non-conducting lesions in the endocardial wall [2, 3]. Pulmonary vein isolation to eliminate triggers is the mainstay of catheter ablation of paroxysmal AF. However, treatment of persistent AF requires modification of a highly re-modeled substrate and this is still currently based on empiricism with success rates being modest, due to the lack of mechanistic understanding of how this arrythmia is perpetuated. The eludication of these mechanisms is challenging to identify from clinically acquired electroanatomic mapping alone.

Computer modelling has the potential to significantly aid clinical intervention in these complex cases and complement existing clinical diagnostic practice. In the majority of organ-scale models of the heart the bidomain, or its monodomain reduction, is used to simulate electrical propagation which can incorporate tissue heterogeneity through a conductivity tensor. Conductivity may be spatially varied to capture localised characteristics of the tissue, such as fibrosis and fibre orientation. Although some of this information may be captured using imaging modalities, translating it into a verifiable and quantifiable form suitable for integration into a computer model is difficult.

Late-gadolinium enhanced magnetic resonance imaging (LGE-MRI) has been used to delineate regions of scar and fibrosis in the left atrium, identified by areas of higher image intensity, following an injection of a gadolinium contrast agent, due to its variable wash out kinetics from scarred myocardium. In recent studies, patients have been classified in one of four Utah categories determined by the percentage of left atrial fibrosis within the LA wall volume: Stage 1 (minimal), Stage 2 (mild), Stage 3 (moderate), and Stage 4 (extensive) [4]. However, to the authors' knowledge, no attempt to date has been made to quantify the relationship between image intensity and model conductivity in such a way as to directly integrate LGE-MRI data into a computer model. In this study, we focus on developing a technique to relate image intensity with conduction velocity (CV) during paced or sinus rhythm.

2. Methods

Both magnetic resonance images and electrical recordings are used in the analysis. Electroanatomic mapping technology records both electrical and spatial positioning data from the electrodes on a multi-pole mapping catheter. Prior to gathering electrical data, the catheter is systematically moved within the chamber to construct a surface representation of the chamber walls using the electrode location data [5, 6]. Sequential mapping records electrical data from electrodes in contact with the chamber wall, from which local activation times (LATs) can be computed relative to a second signal from a fixed-position electrode. The regular rhythm enables the sequentially recorded data to be assembled into a local activation map which is subsequently interpolated and displayed on the chamber geom-

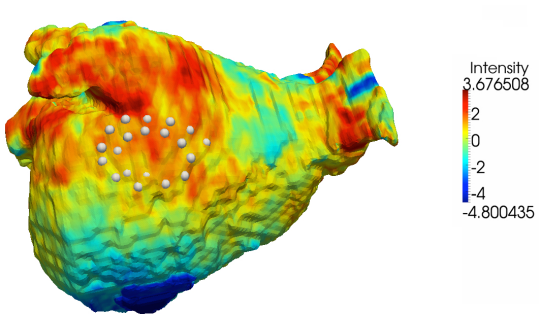

Figure 1. Map of maximum LGE-MRI intensities from 3mm interior of the endocardial surface segmentation, normalised by the standard deviation of the blood pool intensity. High intensity regions are considered representative of areas of fibrosis. Grey dots represent electrode locations.

etry creating an electro-anatomical map [1].

To illustrate the method developed in this paper, endocardial patient data were collected using a 20-electrode AFocusII high-density mapping catheter which was placed in tangential contact with several regions of the left atrial chamber wall, including the roof and the posterior wall. For each position, the chamber was paced from both the coronary sinus and the roof at four cycle lengths (250ms, 300ms, 450ms and 600ms). In total, 32 data sets were collected from one patient. The endocardial surface and electrical recordings were exported for further processing and analysis.

A magnetic resonance angiography (MRA) image of the left atrium blood pool was segmented based on intensity, from which an endocardial surface triangulation was generated. After manual identification of anatomical points on both surfaces, landmark registration was performed using an affine transformation [7]. A subsequent non-rigid surface registration, initialised from the landmark registration, provided the transformation to map the electrode locations onto the MRA surface [8].

An LGE-MRI image of the left atrium was registered to the MRA image using the Image Registration ToolKit [8]. The maximum intensity along a 3mm inward-facing normal to the MRA surface was assigned to the vertices of the triangulation. Intensities were centred around the mean blood pool intensity and normalised by the standard deviation of the blood pool intensity. Regions of the atrium with intensities greater than the mean blood pool intensity were considered to represent scarred tissue [9]. Figure 1 shows an illustrative scar map of the left atrial posterior wall. Higher intensities can be observed on the roof and around the pulmonary veins. Representative transformed endocardial electrode locations for a multi-pole catheter are also identified.

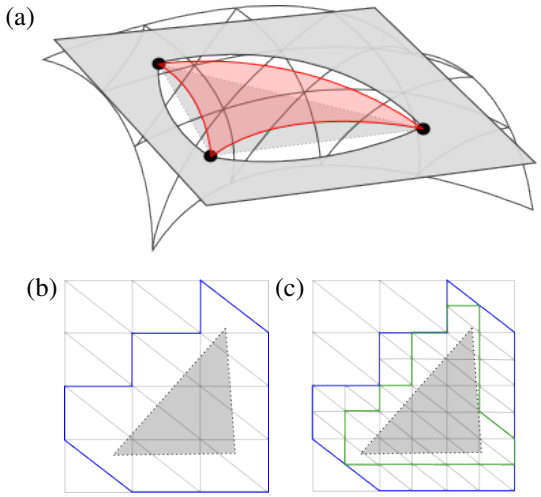

Figure 2. Weighted intensity algorithm: (a) Plane through electrode locations forming triangle; (b) surface mesh projected onto plane and mesh triangles intersecting electrode triangles identified; (c) subdivision of localised mesh.

2.1. CV and LGE-MRI intensity

This study aims to identify if a correlation exists between the LGE-MRI intensity and conduction velocity, as estimated from electroanatomic mapping data. Our analysis combined three algorithms:

- Constrained selection of electrode location triplets;
- Conduction speed estimation for each electrode triplet;
- Estimation of LGE-MRI intensity per unit area for each electrode triplet.

Triplets of electrode locations corresponding to a single catheter were generated such that the resulting triangles had edge lengths within a specific range (15-20mm) and the circumcircle area to triangle area ratio was less than 10. Triangles were permitted to overlap and, on average, this would produce six triangles per catheter.

The average conduction speed across each triangle was estimated using an existing algorithm [10]. Local activation times (LATs) were acquired from the electroanatomic mapping data after manual review by an experienced electrophysiologist. An additional constraint was imposed such that the difference in LAT between at least one pair of electrodes in a given triplet must exceed 3ms. Triplets which did not meet this criterion were rejected.

The average intensity per unit area of a given electrode triplet was computed as follows. A bounding box was first formed containing the electrode triangle and the enclosed surface mesh elements were extracted. These elements were projected onto the plane containing the electrode triangle (Figure 2 (a)). For those triangles intersecting the electrode triangle, the mid-point of each edge was determined and the triangle subdivided into four triangles

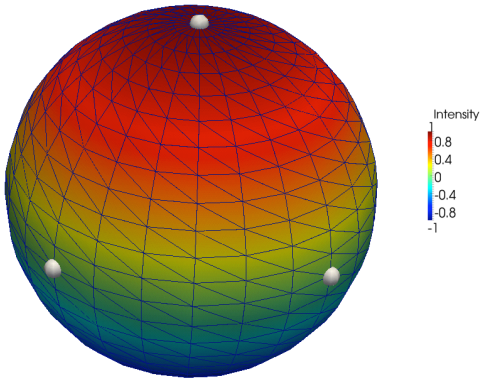

Figure 3. Unit sphere geometry used for validation with prescribed intensity $f(x, y, z) = z$. The three recording virtual electrodes are denoted by grey spheres.

Table 1. Comparison of exact and numerical results for the integration of the intensity over the virtual electrode triangle.

Function	Exact	Numerical	Magnitude Error
$f = 1$	$\pi/2$	1.591	0.020
$f = z$	$\pi/4$	0.784	0.001

(Figure 2 (b,c)). Intensities at the mid-points were linearly interpolated and the process repeated until a desired level of accuracy was achieved. Using vector analysis, it was determined which mesh elements lay entirely within each triangle. These triangles were mapped back to the surface mesh and the weighted intensity per unit area of these triangles was calculated.

3. Results

The algorithm was first validated using two test cases with analytic solutions on the unit sphere using two intensity functions f_i prescribed on the surface. An example is shown in Figure 3. Three points, $(1, 0, 0)$, $(0, 1, 0)$ and $(0, 0, 1)$, were chosen on the sphere to represent a triangular region, with surface area $\pi/2$, and the average intensity function f_i within the triangle was calculated using the algorithms outlined above. The exact integral of the f_i can be computed using spherical coordinates as

$$\int_0^{\pi/2} \int_0^{\pi/2} f_i(\theta, \phi) \sin\phi \, \mathrm{d}\phi \, \mathrm{d}\theta.$$

The integral evaluated numerically using the proposed algorithm was compared with this exact solution, as shown in Table 1.

To illustrate the use of the algorithms, we applied it to clinical electrogram and imaging data collected from

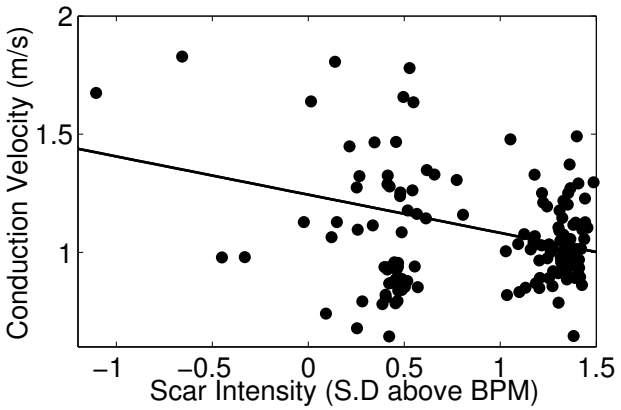

Figure 4. Calculated normalised intensity and CV across all the electrode triangles for the clinical data.

Table 2. Correlation properties for different cycle lengths.

	250ms	300ms	400ms	600ms
gradient	-0.091	-0.039	0.032	-0.17
y-intercept	1.08	1.15	0.93	1.38
r	-0.265	-0.695	0.1004	-0.4070
p	N.S.	N.S.	N.S.	< 0.05

a single patient. Figure 4 shows the calculated CVs and LGE-MRI intensities for all triangles with edge lengths of 15-20mm. The calculated conduction velocities were within a physiological range of 0.6 to 1.81m s^{-1}. The data has a negative Pearson's r-correlation coefficient of $r = -0.2254$, suggesting decreasing CV with increasing LGE-MRI intensity. This was found to be statistically significant ($p < 0.05$) based on a students t-test.

Since CV is dependent on paced cycle length, the results from individual cycle lengths were analyzed separately. Figure 5 shows the calculated CV and LGE-MRI intensities (normalised by the SD of the mean blood pool intensity) for each cycle length. For three of the four cycle lengths, we still see a negative correlation (Table 2) although, due to the reduction in the volume of data, the correlation is only statistically significant for a CL=600ms.

4. Discussion

We have developed a method which computes the average underlying scar intensity derived from the LGE-MRI of the left atrium and enabled a direct localised comparison with the corresponding conduction velocity of electrical propagation in the tissue. The method has been validated and strong agreement is found with analytical results (maximum relative error of 0.01%) .

The algorithm was then applied to data gathered from a patient, through MRI and electroanatomic mapping, prior

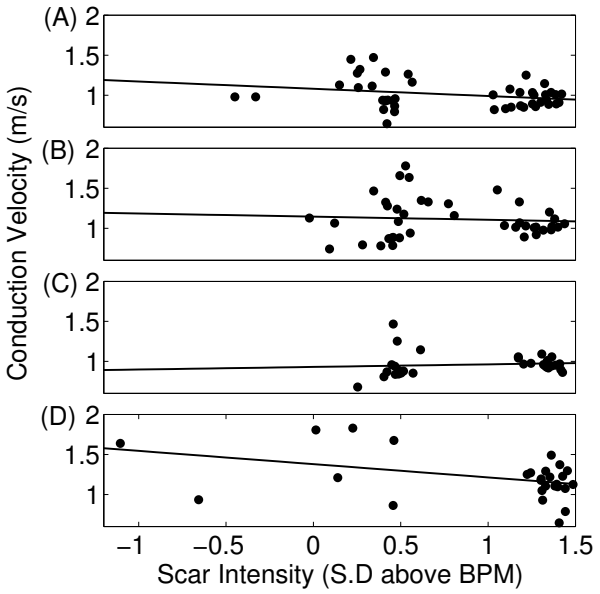

Figure 5. Standard Deviation of scar intensity vs. Conduction Velocity for different cycle lengths. A: CL=250ms, B: CL=300ms, C: CL=400ms and D: CL = 600ms

to catheter ablation where the data suggest there is a negative correlation between the LGE-MRI intensity, normalised by the SD of the mean blood pool intensity, and CV.

Error is potentially accumulated during several stages of the algorithm. This includes registration of the MRA with the LGE-MRI images, as well as the segmentation of the MRA image itself. An error may also occur during the registration of the endocardial geometry obtained from electro-anatomical mapping onto the MRI surface, due to the difference in morphology between the two datasets and the choice of landmark points, which affects both the computed average intensity and CV. We estimate our registration error to be less than 3mm, and as such have chosen triangles with edge lengths between 15 and 20mm. In this analysis, we have also not been able to account for the underlying anisotropy and fibre direction of the atrial wall.

The present study includes data from only a single patient to demonstrate the use of the algorithm on clinical data. Further work will apply the algorithm to a larger cohort of patients to establish the overall trends which can be then be incorporated into a modelling environment.

Acknowledgements

This work was supported by the British Heart Foundation (BHF), grants FS/11/22/28745 & RG/10/11/28457, the ElectroCardioMaths Programme of the Imperial BHF Centre of Research Excellence and the NIHR Imperial Biomedical Research Centre.

References

[1] Zipes DP, Jalife J. Cardiac Electrophysiology: From Cell to Bedside. W.B. Saunders Company, 2009.

[2] Narayan SM, Krummen DE, Shivkumar K, Clopton P, Rappel WJ, Miller JM. Treatment of Atrial Fibrillation by the Ablation of Localized Sources. JAC 2012;60(7):628–636.

[3] Zlochiver S, Yamazaki M, Kalifa J, Berenfeld O. Rotor meandering contributes to irregularity in electrograms during atrial fibrillation. Heart Rhythm 2008;5(6):846–854.

[4] Oakes RS, Badger TJ, Kholmovski EG, Akoum N, Burgon NS, Fish EN, Blauer JJE, Rao SN, DiBella EVR, Segerson NM, Daccarett M, Windfelder J, McGann CJ, Parker D, MacLeod RS, Marrouche NF. Detection and quantification of left atrial structural remodeling with delayed-enhancement magnetic resonance imaging in patients with atrial fibrillation. Circulation April 2009;119(13):1758–67. ISSN 1524-4539.

[5] Earley MJ, Showkathali R, Alzetani M, Kistler PM, Gupta D, Abrams DJ, Horrocks JA, Harris SJ, Sporton SC, Schilling RJ. Non-fluoroscopic mapping systems for electrophysiology: the 'tool or toy' dilemma after 10 years. European Heart Journal 2005;27(10):1134–1136.

[6] Eitel C, Hindricks G, Dagres N, Sommer P, Piorkowski C. EnSite Velocity cardiac mapping system: a new platform for 3D mapping of cardiac arrhythmias. Exper Rev Med Devices 2010;7(2):185–192.

[7] Studholme,C and Hill,D L G, Hawkes DJ. An overlap invariant entropy measure of 3D medical image alignment. Pattern Recognition 1999;32(1):71–86.

[8] Rueckert D, Sonoda LI, Hayes C, Hill DL, Leach MO, Hawkes DJ. Nonrigid registration using free-form deformations: application to breast MR images. IEEE transactions on medical imaging August 1999;18(8):712–21. ISSN 0278-0062.

[9] Malcolme-Lawes LC, Juli C, Karim R, Bai W, Quest R, Lim PB, Jamil-Copley S, Kojodjojo P, Ariff B, Davies DW, Rueckert D, Francis DP, Hunter R, Jones D, Boubertakh R, Petersen SE, Schilling R, Kanagaratnam P, Peters NS. Automated analysis of atrial late gadolinium enhancement imaging that correlates with endocardial voltage and clinical outcomes: a 2-center study. Heart rhythm the official journal of the Heart Rhythm Society August 2013; 10(8):1184–91. ISSN 1556-3871.

[10] Kojodjojo P, Kanagaratnam P, Markides V, Davies DW, Peters N. Age-related changes in human left and right atrial conduction. Journal of cardiovascular electrophysiology February 2006;17(2):120–7. ISSN 1045-3873.

Address for correspondence:

Rheeda Ali
Department of Bioengineering, Imperial College London, SW7 2AZ
rheeda.ali07@imperial.ac.uk